Heliyon 10 (2024) e33359

Contents lists available at ScienceDirect

Heliyon

journal homepage: www.cell.com/heliyon

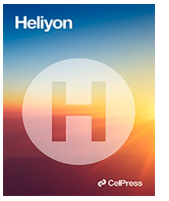

Research article

Computational identification of novel potential genetic pathogenesis and otherwise biomarkers in acute liver allograft rejection

Cheng Zhang [a,1], Jun-Ze Chen [a,1], Kun Dong [a,1], Yong-Yuan Jian [a], Kai-Yong Huang [a], Rui-Ling Su [a], Xue-Lin Tan [a], Guan-Dou Yuan [b,c,d], Yu-yan Lan [e], Song-Qing He [b,c,d,**], Chun-Qiang Dong [a,*]

[a] *Department of Organ Transplantation, the First Affiliated Hospital of Guangxi Medical University, Nanning, Guangxi, China*
[b] *Department of Hepatobiliary Surgery, the First Affiliated Hospital of Guangxi Medical University, Nanning, Guangxi, China*
[c] *Key Laboratory of Early Prevention and Treatment for Regional High-Frequency Tumor (Guangxi Medical University), Ministry of Education, Nanning, Guangxi, China*
[d] *Guangxi Key Laboratory of Immunology and Metabolism for Liver Diseases, Nanning, Guangxi, China*
[e] *Department of Anesthesiology, the First Affiliated Hospital of Guangxi Medical University, Nanning, Guangxi, China*

ARTICLE INFO

Keywords:
Liver transplantation
Acute cellular rejection
Biomarkers
Mechanisms
Hub genes

ABSTRACT

Acute cellular rejection (ACR) is a prevalent postoperative complication following liver transplantation (LT), exhibiting an increasing incidence of morbidity and mortality. However, the molecular mechanisms of ACR following LT remain unclear. To explore the genetic pathogenesis and identify biomarkers of ACR following LT, three relevant Gene Expression Omnibus (GEO) datasets consisting of data on ACR or non-ACR patients after LT were comprehensively investigated by computational analysis. A total of 349 upregulated and 260 downregulated differentially expressed genes (DEGs) and eight hub genes (*ISG15, HELZ2, HNRNPK, TIAL1, SKIV2L2, PABPC1, SIRT1, and PPARA*) were identified. Notably, *HNRNPK*, *TIAL1*, and *PABPC1* exhibited the highest predictive potential for ACR with AUCs of 0.706, 0.798, and 0.801, respectively. KEGG analysis of hub genes revealed that ACR following LT was predominately associated with ferroptosis, protein processing in the endoplasmic reticulum, complement and coagulation pathways, and RIG-I/NOD/Toll-like receptor signaling pathway. According to the immune cell infiltration analysis, γδT cells, NK cells, Tregs, and M1/M2-like macrophages had the highest levels of infiltration. Compared to *SIRT1, ISG15* was positively correlated with γδT cells and M1-like macrophages but negatively correlated with NK cells, $CD4^+$ memory T cells, and Tregs. In conclusion, this study identified eight hub genes and their potential pathways, as well as the immune cells involved in ACR following LT with the greatest levels of infiltration. These findings provide a new direction for future research on the underlying mechanism of ACR following LT.

* Corresponding author. the First Affiliated Hospital of Guangxi Medical University, Nanning, China.
** Corresponding author. the First Affiliated Hospital of Guangxi Medical University, Nanning, China.
E-mail addresses: dr_hesongqing@163.com (S.-Q. He), dongchunqiang@163.com (C.-Q. Dong).
[1] These authors have contributed equally to this work and share first authorship.

https://doi.org/10.1016/j.heliyon.2024.e33359
Received 16 November 2023; Received in revised form 20 May 2024; Accepted 19 June 2024
Available online 22 June 2024

1. Introduction

Acute liver allograft rejection can be categorized into acute cellular rejection (ACR) and antibody-mediated rejection (AMR). It remains an important cause of allograft dysfunction, with an estimated ACR incidence of 10–30 % in LT recipients [1,2], while AMR has a lower incidence (approximately 1 %) in LT recipients [3]. ACR is associated with an increased risk of graft loss, graft failure-related death, and all-cause mortality [1,4]. Predicting acute rejection is challenging, and diagnosis requires an invasive liver biopsy, remaining the gold standard [4]. However, this procedure is commonly associated with complications (e.g., pain, hemorrhage, and biliary leakage) and is prone to sampling issues [5,6]. Unfortunately, due to the unclear mechanism of ACR following LT, it is difficult to develop a precise anti-rejection therapeutic regimen [7,8]. Recently, the discovery of omics-based biomarkers has provided new insights into identifying novel mechanisms and therapeutic targets of organ transplant rejection [9]. Any difference in the histocompatibility antigens between the donor and the recipients can potentially trigger an immune response, which may subsequently lead to ACR [10–12]. Therefore, it is crucial to profile and analyze changes in the immune microenvironment of the transplanted livers and alterations in gene expression modulating immune cell infiltration for their relevance to the ACR following LT.

In this study, we performed a preliminary computational analysis and applied various bioinformatics tools to integrate omics data to elucidate the genetic pathogenesis and novel biomarkers associated with ACR following LT. Our findings can provide comprehensive insights into the pathogenesis and therapeutic targets of ACR following LT, as well as preliminary data for future research on genetic and molecular mechanisms.

2. Materials and methods

In silico analysis.

2.1. Dataset collection

We searched the Gene Expression Omnibus (GEO) database from NCBI (https://www.ncbi.nlm.nih.gov/geo/) using the following keywords: ("liver transplantation" OR "liver transplant*" OR "liver graft*") AND (acute rejection OR "graft failure" OR "liver failure" OR "acute graft rejection" OR "acute allograft rejection" OR "acute liver allograft rejection"). Afterward, the title and abstract of the publications were screened.

Inclusion criteria for datasets are as follows: 1. GEO datasets from patients who only underwent LT and either experienced or did not experience acute rejection; 2. The sequencing data originated from a needle biopsy of transplanted liver tissue; 3. Rejection occurred before immunosuppression was completely discontinued. Exclusion criteria: 1. Combined organ or multi-organ transplant patients; 2. GEO datasets from animal experiments; 3. Chronic rejection or AMR of LT.

2.2. Data normalization and differential expression analysis

Before differential expression analysis, the raw gene expression data of the eligible GEO datasets were normalized using the R package "preprocessCore." After pre-processing, the differentially expressed genes (DEGs) were screened with a threshold of P-value <0.05 and $|\log2 \text{ fold-change (FC)}| > 0$ using the "limma" package. By Venn diagram analysis, genes up- or down-regulated simultaneously in at least two datasets were selected as DEGs for subsequent analysis.

2.3. Enrichment analysis

To identify possible functions and pathways, we conducted functional enrichment analysis of DEGs using the R package "clusterProfiler," including Gene Ontology (GO) terms and the Kyoto Encyclopedia of Genes and Genomes (KEGG) pathways. Subsequently, the results were visualized using the clusterProfiler.

2.4. Weighted gene co-expression network analysis (WGCNA)

The gene co-expression networks and gene modules of DEGs were constructed using the R package "WGCNA" and a hierarchical clustering dendrogram. Subsequently, genes exhibiting similar expression patterns were divided into different modules, and the expression profiles of each module were summarized using the module eigengene (ME). Finally, the correlation between the ME modules and ACR following LT was explored. Genes in modules showing a high correlation coefficient with ACR following LT were selected to construct a protein-protein interaction (PPI) network.

2.5. PPI network analysis and hub gene recognition

Key genes from WGCNA were input to the STRING (https://string-db.org/) database to build a PPI network, which was then visualized using Cytoscape software. The CytoHubba plugin within Cytoscape was employed to identify hub genes. Three algorithms (Betweenness, Closeness, and Stress) were used to identify the 10 hub genes, each defined as a core gene of the PPI network. To identify the most relevant hub genes, a Venn diagram analysis was performed to determine the intersection of the top 10 hub genes ranked by all three algorithms.

2.6. Immune infiltration analysis

The infiltration levels of immune cells were evaluated using the R package "CIBERSORT" (https://cibersort.stanford.edu/). Additionally, the correlation between hub genes and immune cell infiltration levels was explored.

2.7. Statistical analysis

All statistical and bioinformatics analyses were conducted using R software (version 4.1.1) and its program packages. P-value <0.05 was considered statistically significant.

3. Results

3.1. Baseline information of the eligible GEO datasets

According to the inclusion criteria, the GSE26622, GSE26625, and GSE52420 datasets were included [13,14], including 97 liver biopsy samples consisting of 45 non-ACR and 52 ACR LT recipients' samples. The mRNA expression profiles and clinical information of these datasets were extracted for further analysis. All details are shown in Table 1.

3.2. Identification of DEGs

After normalizing the mRNA expression data (Figs. S1(a–f)), a total of 723 up- and 225 down-regulated DEGs were identified in GSE26622, 2787 up- and 2962 down-regulated DEGs in GSE26625, and 1671 up- and 1884 down-regulated DEGs in GSE52420 through differential expression analysis. The volcano plots and heat maps of the top 10 up- and down-regulated genes across three datasets are shown in Fig. S2. As expected, Venn diagram analysis revealed 349 up- and 260 down-regulated DEGs in the ACR groups of three datasets (Fig. 1(a–b)). The complete list of the identified DEGs is shown in Tables S1–S4.

3.3. Functional enrichment analysis

The identified DEGs were functionally enriched for possible biological functions. GO analysis showed that DEGs were mainly related to cell growth, positive regulation of the catabolic process, macroautophagy, the vacuolar membrane, the mitochondrial matrix, and ribonucleoside binding (Fig. 2(a–c)). The KEGG analysis showed significant enrichment of genes involved in the phagosome, oxidative phosphorylation, autophagy, ferroptosis, drug metabolism, steroid hormone biosynthesis, and amino acid metabolism in ACR following LT (Fig. 2(d)). The complete list of GO terms and KEGG pathways for the identified DEGs is shown in Table S5.

3.4. Weighted gene co-expression network analysis and identification of key modules

To identify key gene functional modules associated with ACR following LT, WGCNA was further conducted in GSE26625, which had the largest sample size among the three datasets. The distribution of the clinical characteristics in the samples from GSE26625 is illustrated in Fig. S3(a). Seven was determined to be the best soft threshold (Fig. S3(b)). After merging similar modules (Fig. S3(c)), three modules were obtained, namely, ME-blue, ME-turquoise, and ME-grey modules (Fig. 3). The ME-blue module exhibited a positive correlation with ACR features of LT patients (Fig. 3(a–d)). Subsequently, GO and KEGG pathway analyses were conducted based on the DEGs in the three modules (Table S6). KEGG pathway analysis in the three modules revealed that the ME-blue module was associated with pathways of Ribosome, Phagosome, Drug metabolism, and Steroid hormone biosynthesis (Fig. 4(a)). Neurodegeneration, Synaptic vesicle cycle, and Autophagy passways were associated with the ME-turquoise module (Fig. 4(b)). Moreover, the p53 signaling pathway, Endocytosis, and Axon guidance exhibited associations with the ME-grey module (Fig. 4(c)). Fig. 4(d–f) also shows the association of DEGs with the top 5 KEGG terms in each module. In this study, genes in the ME-blue module having a significant positive correlation with clinical features of ACR following LT were selected for subsequent analysis.

Table 1
Characteristics of the three GEO datasets.

GEO accession	Author	Platform	Samples (Non-ACR: ACR)	Year	Country
GSE26622	Bohne F	GPL570[HG-U133_Plus_2] Affymetrix Human Genome U133 Plus 2.0 Array	9:10	2012	Italy, Germany, Spain, Belgium, the Netherlands
GSE26625	Bohne F	GPL6947 Illumina Human HT-12 V3.0 Expression BeadChip	24:29	2012	Italy, Germany, Spain, Belgium, the Netherlands
GSE52420	Bohne F	GPL10558 Illumina Human HT-12 V4.0 Expression BeadChip	12:13	2014	Germany, Spain

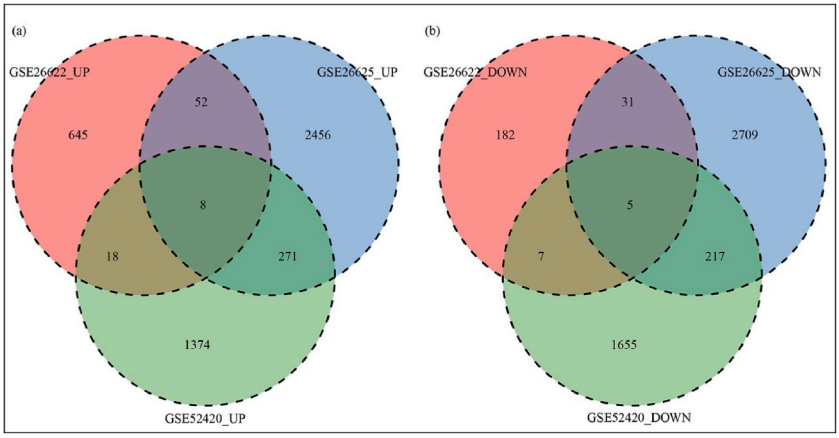

Fig. 1. Venn diagrams analysis of DEGs in three datasets. (a) A total of 349 upregulated DEGs in the ACR groups of three datasets were identified by intersecting with Venn diagrams analysis. (b) A total of 260 down-regulated DEGs in the ACR groups of three datasets were identified by intersecting with Venn diagrams analysis. $|\log2FC| > 0$ and P-value <0.05 were set as the threshold values.

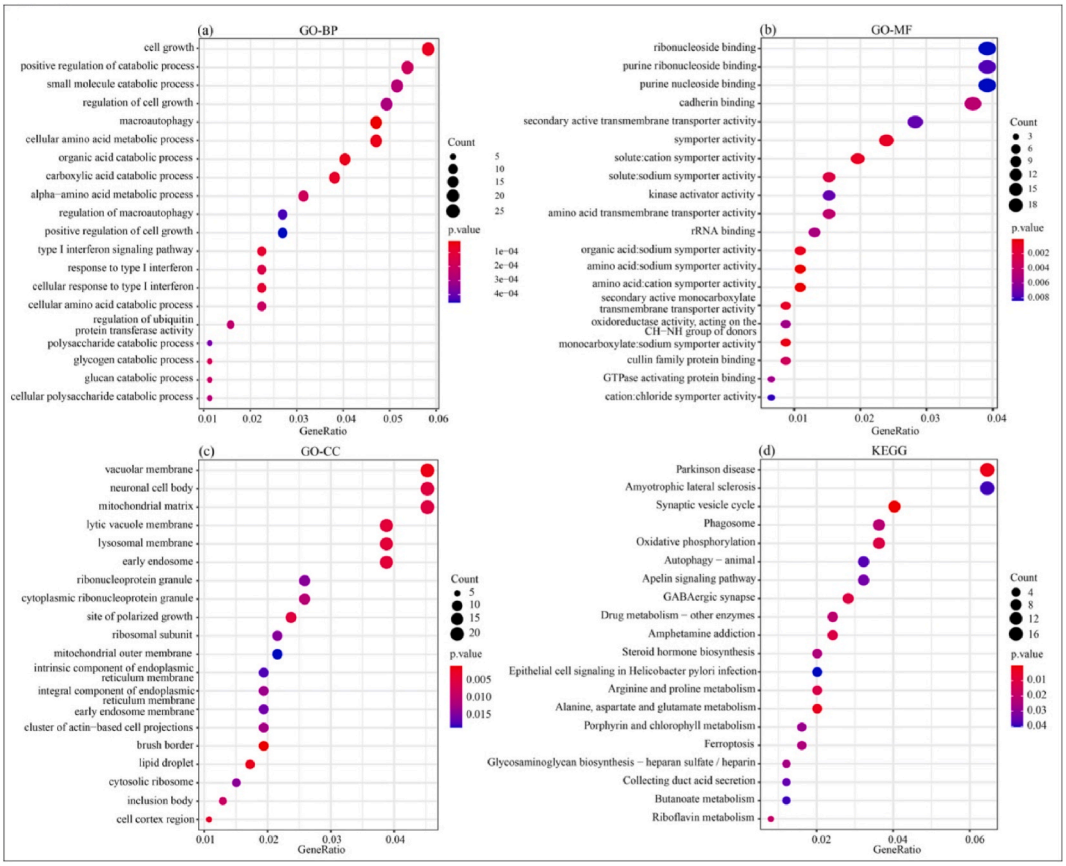

Fig. 2. Functional enrichment on the identified DEGs. (a–c) The top 20 terms of biological process (BP) terms, molecular function (MF) terms, and cellular component (CC) terms of DEGs identified by GO analysis. (d) The top 20 terms of KEGG pathways of DEGs identified by KEGG pathway analysis.

3.5. Protein-protein interaction network construction and identification of hub genes

The PPI network of DEGs in the ME-blue module was constructed using the STRING database (Fig. S4). Then, the top 10 hub genes were identified using three algorithms (Betweenness, Closeness, and Stress) available in the cytoHubba (Fig. 5(a–c)). To identify the

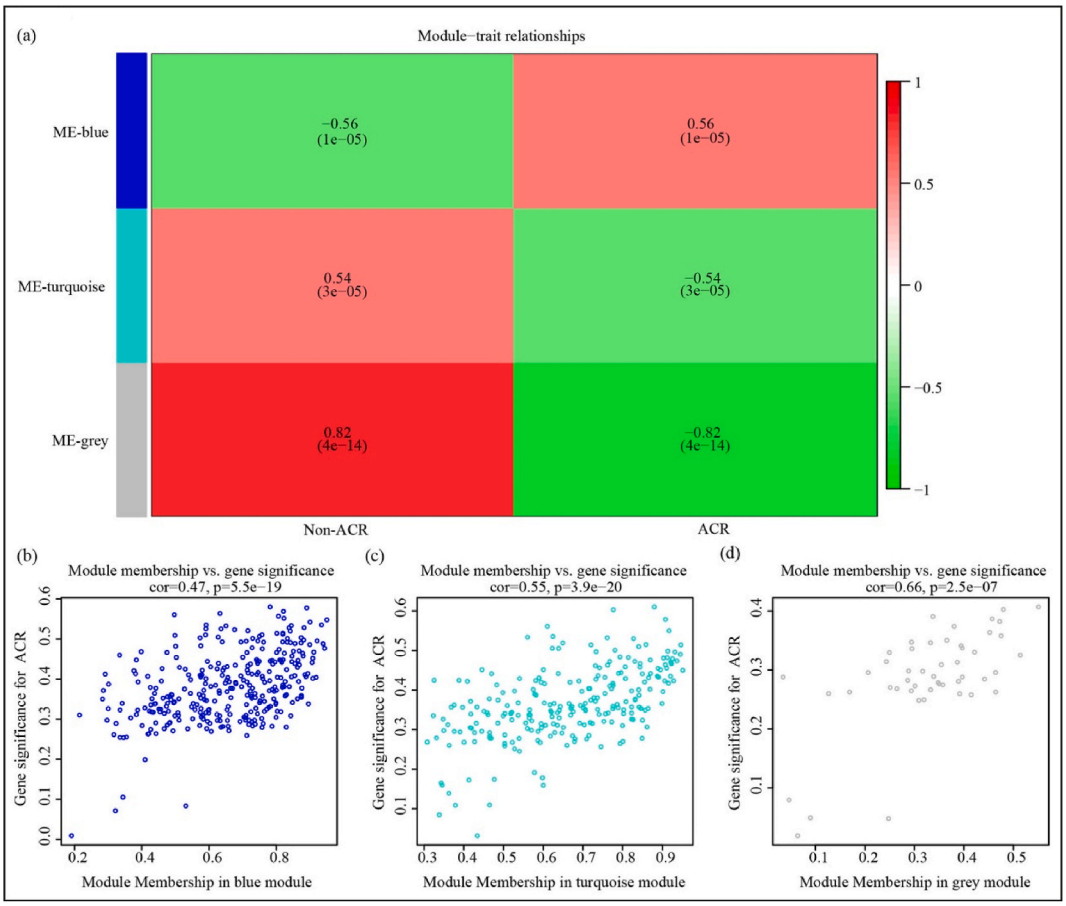

Fig. 3. Identification of key modules via WGCNA in GSE26625. (a) Three modules (ME-blue, ME-turquoise, and ME-grey modules) and the module-trait relationships of the three modules were identified via WGCNA. (b–d) The correlation of gene significance with ACR features and indicated module membership.

most relevant hub genes, the top 10 hub genes ranked by all three algorithms were intersected through Venn diagrams analysis. Finally, only eight overlapped hub genes were identified, namely, *ISG15*, *HELZ2* (also known as *RPIC285*), *HNRNPK* (also known as *HNRPK*), *TIAL1*, *SKIV2L2*, *PABPC1*, *SIRT1*, and *PPARA* (Fig. 5(d)). Fig. 6(a) shows the log2FC of each gene in GSE26622, GSE26625, and GSE52420, and the correlation of the eight hub genes was further examined using these three datasets (Fig. 6(b–d)). The results indicated a downregulation of *ISG15* and *HELZ2* in the rejection group, while *SKIV2L2*, *SIRT1*, and *PPARA* exhibited an upregulation in all three GEO datasets. Moreover, *HNRNPK*, *TIAL1*, and *PABPC1* were upregulated in the ACR group in GSE26625 and GSE52420 but were downregulated in GSE26622. *ISG15* was positively correlated with *HELZ2* but negatively correlated with the other six genes in all three datasets (Fig. 6(b–d)). Finally, receiver operating characteristic (ROC) analysis was performed to evaluate the efficiency of the eight hub genes for predicting the ACR event. *HNRNPK*, *TIAL1*, and *PABPC1* exhibited the highest predictive potential, with AUCs of 0.706, 0.798, and 0.801 in GSE26622, GSE26625, and GSE52420 (Fig. 6(e–g)), respectively.

3.6. Immune cell infiltration analysis

We subsequently analyzed the immune cell infiltration in tissues obtained from GSE26625, which had the largest sample size (Fig. 7). Moreover, the correlation between hub genes and various immune cells was analyzed, including NK cells, memory B cells, $CD4^+$ memory T cells, T regulatory cells (Tregs), naïve B cells, neutrophils, mast cells, dendritic cells, and M1/M2-like macrophages (Fig. 7(a)). Interestingly, the levels of *SKIV2L2* encoding mRNA were positively associated with amount of resting NK cells but negatively associated with amount of activated NK cells and resting mast cells (Fig. 7(b)). The levels of *ISG15* encoding mRNA exhibited a positive correlation with amount of γδT cells, M1-like macrophages, and activated dendritic cells but a negative correlation with amount of resting NK cells, resting $CD4^+$ memory T cells, and Tregs (Fig. 7(c)). The levels of *HELZ2* encoding mRNA were positively correlated with amount of γδT cells, activated dendritic cells, and M1-like macrophages but negatively correlated with amount of M2-like macrophages, resting NK cells, and neutrophils (Fig. 7(d)). The levels of *HNRNPK* encoding mRNA were positively correlated with amount of resting $CD4^+$memory T cells (Fig. 7(e)). The levels of both *TIAL1* and *PPARA* encoding mRNA were

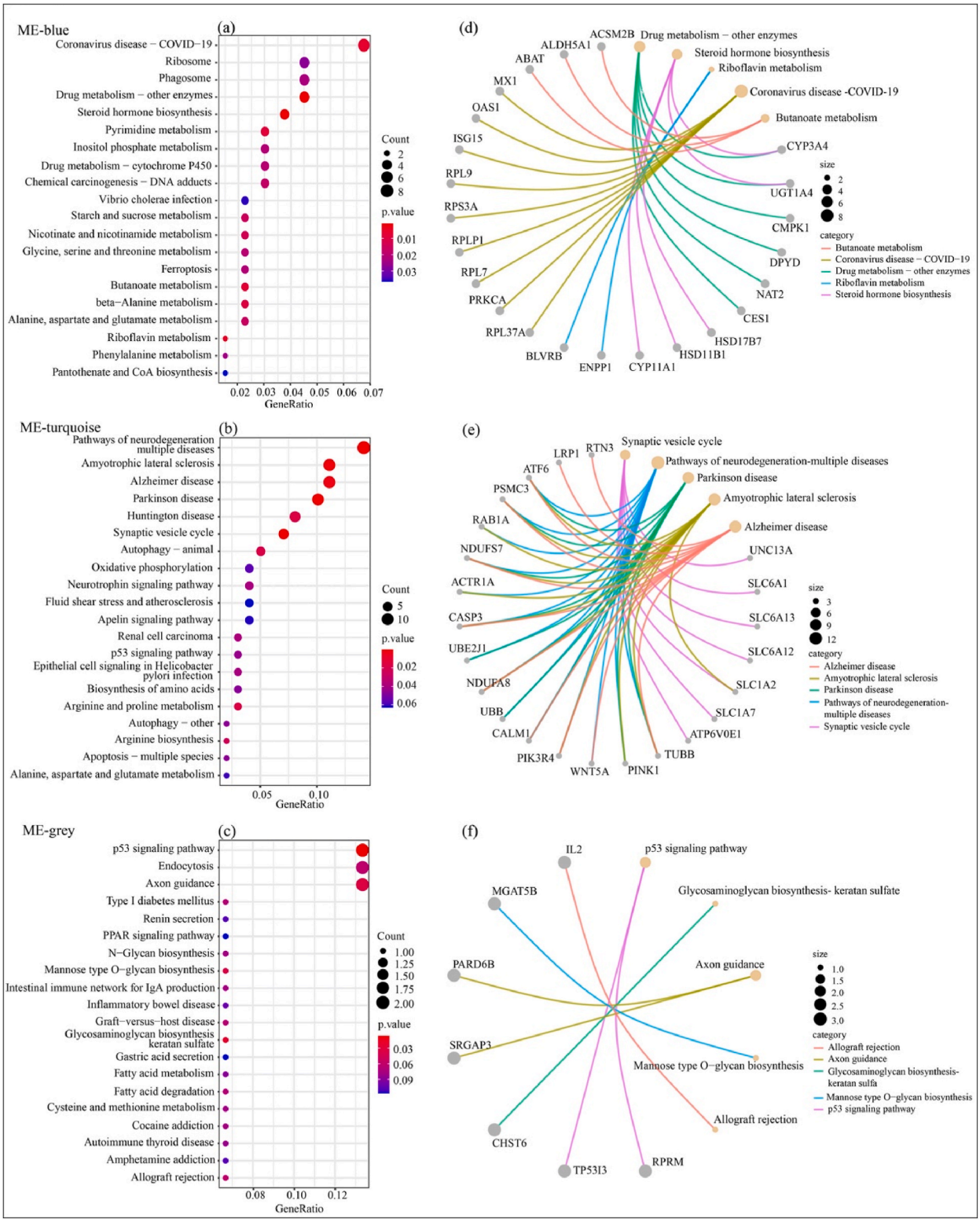

Fig. 4. KEGG pathway analysis of DEGs from three key modules. (a–c) The top 20 terms of KEGG pathways of DEGs from ME-blue, ME-turquoise, and ME-grey, respectively. (d–f) The association of DEGs with top 5 KEGG terms from ME-blue, ME-turquoise, and ME-grey, respectively.

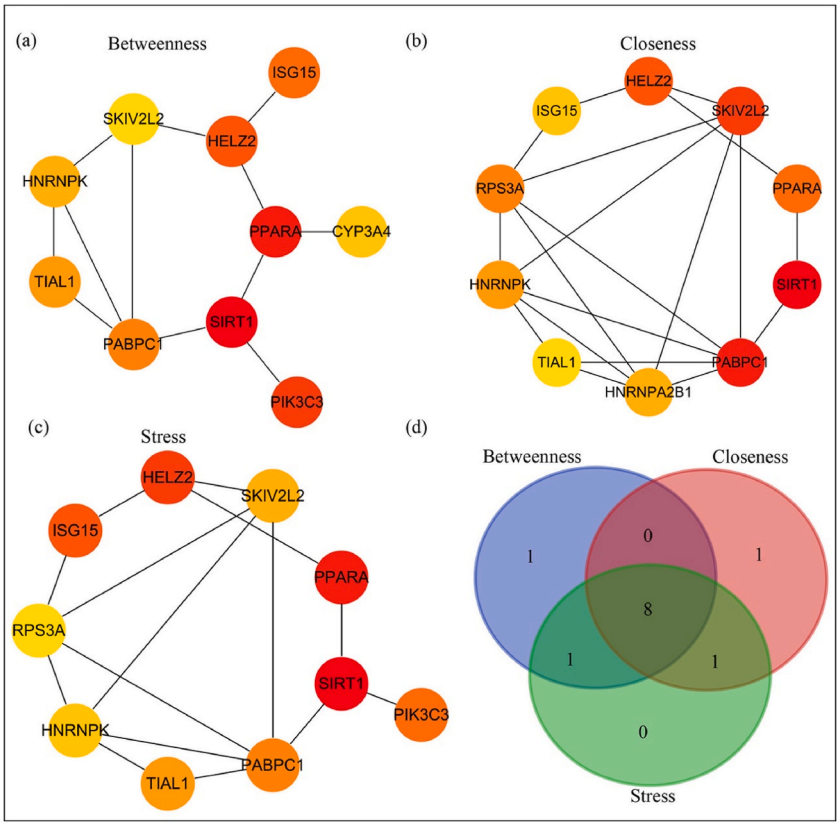

Fig. 5. Identification of hub genes. (a–c) The top 10 hub genes identified using different algorithms in cytoHubba, including Betweenness (a), Closeness (b), and Stress (c). (d) Eight overlapped genes from three algorithms identified by Venn diagram analysis.

negatively associated with amount of γδT cells. The levels of *TIAL1* encoding mRNA were negatively associated with amount of activated NK cells but positively correlated with amount of Tregs. In contrast, the levels of *PPARA* encoding mRNA were positively correlated with amount of naïve B cells and resting NK cells (Fig. 7(f and g)). The levels of *PABPC1* encoding mRNA were positively correlated with amount of resting NK cells, resting $CD4^+$ memory T cells, and naïve B cells but negatively correlated with amount of γδT cells, M1-like macrophages, and activated NK cells (Fig. 7(h)). The levels of *SIRT1* encoding mRNA were positively correlated with amount of resting NK cells, resting $CD4^+$ memory T cells, Tregs, naïve B cells, neutrophils, and M2-like macrophages but negatively correlated with amount of γδT cells and memory B cells (Fig. 7(i)). The populations of immune cells that exhibited the highest infiltration included $CD4^+$ memory T cells, γδT cells, NK cells, Tregs, and M1/M2-like macrophages. These preliminary data suggest that eight hub genes may drive ACR following LT by regulating immune cell infiltration. However, the underlying regulatory mechanism needs to be further investigated.

3.7. Exploration of hub genes

The correlation between hub genes and all genes in GSE26625 was examined. The heat maps of the top 50 genes with positive correlation are shown in Fig. S5(A–H). Based on the correlation analysis, KEGG pathway analysis was performed, and the top 20 associated pathways correlated with each of the eight hub genes were obtained (Fig. 8). For the top three predictors, *HNRNPK* was closely associated with protein processing in the endoplasmic reticulum, salmonella infection, and ferroptosis (Fig. 8(a)); *TIAL1* demonstrated a significant association with the endoplasmic reticulum, complement and coagulation, and regulation of the actin cytoskeleton (Fig. 8(h)); *PABPC1* displayed a strong correlation with protein processing in the endoplasmic reticulum, complement and coagulation, and ferroptosis (Fig. 8(c)). The KEGG analysis of the eight hub genes revealed that the pathways most associated with ACR following LT were ferroptosis, protein processing in the endoplasmic reticulum, complement and coagulation, and the RIG-I/NOD/Toll-like receptor signaling pathway (Fig. 8(a–h). Ferroptosis was associated with *HNRNPK*, *ISG15*, *PABPC1*, *PPARA*, *SIRT1*, and *SKIV2L2* (Fig. 8(a–d), (f-g)). Protein processing in the endoplasmic reticulum pathway was associated with *HNRNPK*, *ISG15*, *PABPC1*, *PPARA*, *SIRT1*, *SKIV2L2*, and *TIAL1* (Fig. 8(a–d), (f–h)). The complement and coagulation pathways were associated with *HNRNPK*, *PABPC1*, *SIRT1*, and *TIAL1* (Fig. 8(a), (c), (f), and (h)). RIG-I/NOD/Toll-like receptor signaling pathway and antigen processing and presentation pathway were associated with *ISG15* and *HELZ2* (Fig. 8(b), (e)), and a significant correlation was observed between Th17 cell differentiation and *ISG15* (Fig. 8(b)). Autophagy, ribosome, and proteasome were also identified as closely

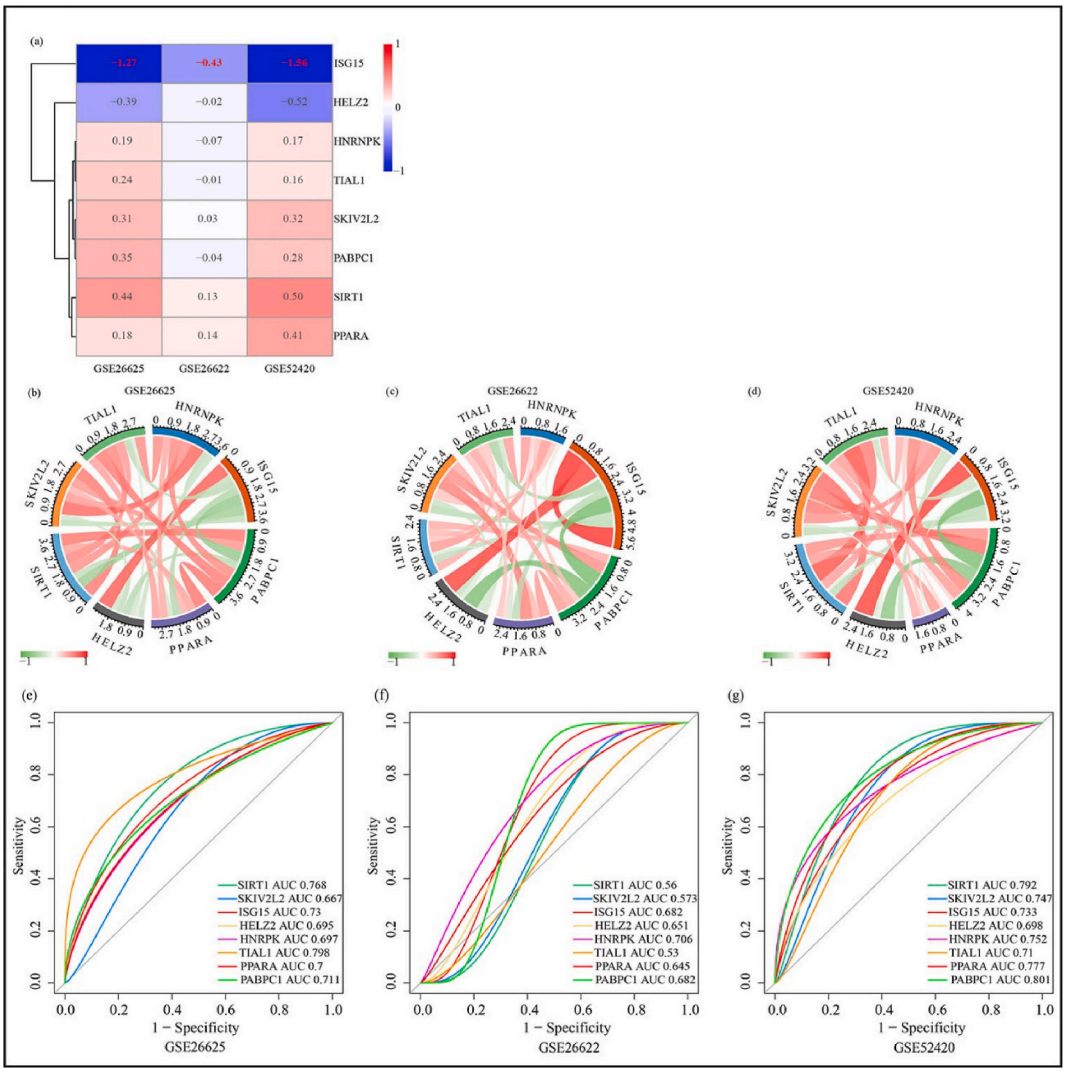

Fig. 6. Validation and ROC curves of the eight hub genes in the indicated GEO datasets. (a) Heat map showing the log2(FC) values of the eight hub genes. Correlation of the eight hub genes in GSE26625 (b), GSE26622 (c), and GSE52420 (d). The red line represents a positive correlation, and the green line represents a negative correlation, with a deeper color indicating a stronger correlation. (e–g) ROC curves reflecting the efficiency of the eight hub genes for predicting the ACR event in the indicated GEO datasets.

associated pathways.

4. Discussion

In this study, we analyzed three datasets related to ACR following LT from the GEO database and obtained 349 up- and 260 down-regulated DEGs in the rejection group. The significant differences in the number of up- and down-regulated genes among the three datasets were identified, which can be attributed to the different sample sizes of each data set, consistent with the findings of Alfaro R [15]. By integrating different sequencing datasets and bioinformatics analysis methods, eight hub genes and their potential pathways, as well as the greatest infiltration immune cells associated with ACR following LT, were mined and identified. No similar reports have been retrieved according to a PubMed literature search. Therefore, applying bioinformatic tools for integrating omics data to uncover the genetic pathogenesis associated with organ transplantation rejection is a valuable research method [15]. Through functional enrichment analysis, potential biological functions related to these DEGs have been identified. Consistent with the results of KEGG analysis, these DEGs were enriched in oxidative phosphorylation, autophagy, and ferroptosis, and the function of autophagy in LT rejection has been extensively investigated [16]. Moreover, ischemic preconditioning has been reported to induce autophagy and limit necrosis in human recipients of fatty liver grafts, decreasing the incidence of rejection episodes [17]. However, the most remarkable finding among these pathways was the ferroptosis pathway, which was first identified in 2012 as an iron-dependent form of oxidative cell death characterized by iron-dependent accumulation of intracellular reactive oxygen species [18]. As an emerging form of

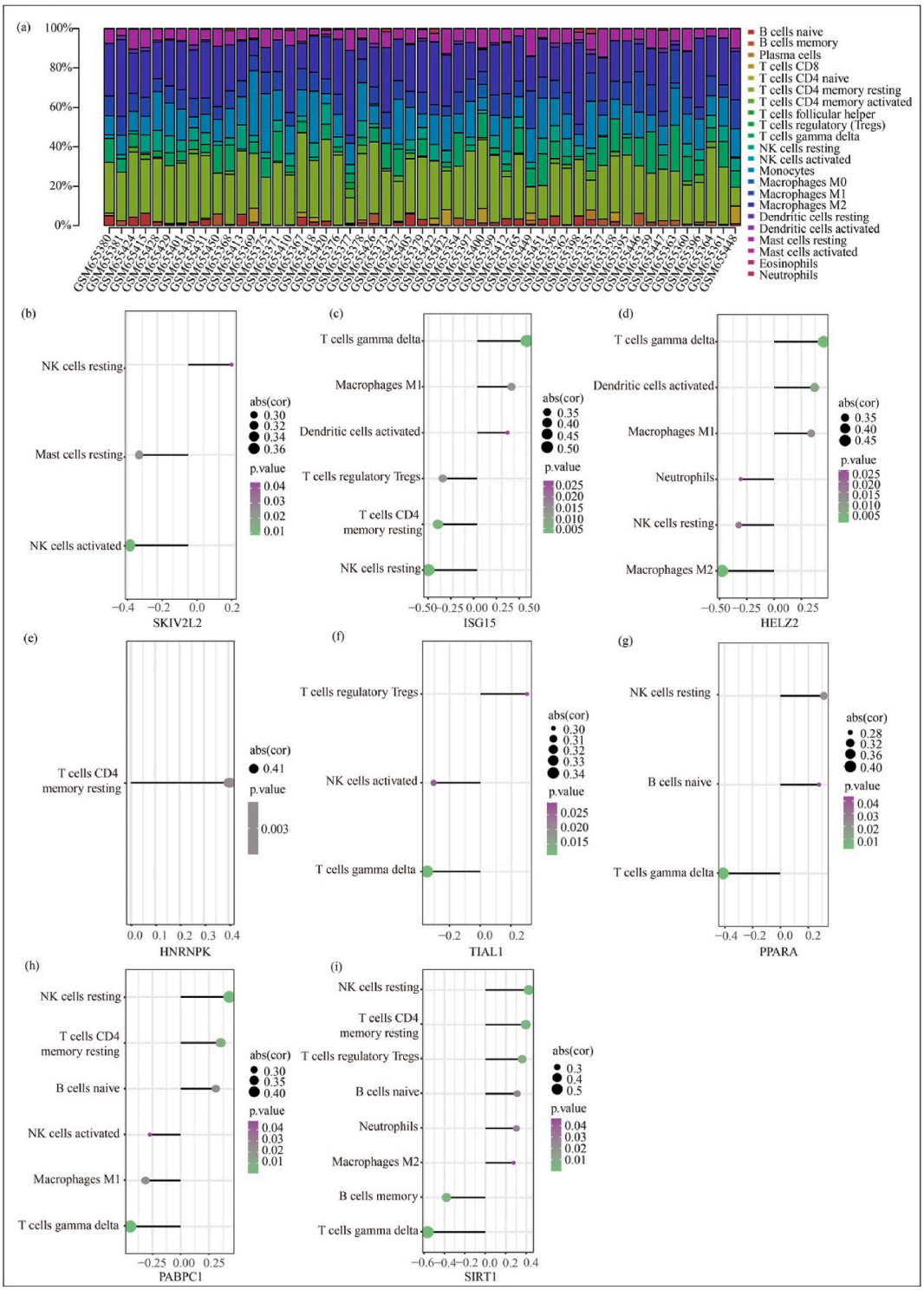

Fig. 7. Results of immune infiltration analysis in tissues from GSE26625. (a) The proportion of indicated immune cells in GSE26625. (b–i) The correlation of the infiltrated immune cells with the indicated hub genes.

programmed cell death, limited studies have confirmed the contribution of ferroptosis to the pathogenesis of hepatic I/R injury during LT [19,20]. Recently, an integrated analysis of omics-based data was conducted to establish a ferroptosis-related gene signature to predict graft loss following allogeneic kidney transplantation based on graft rejection-related genes. The results suggested a close

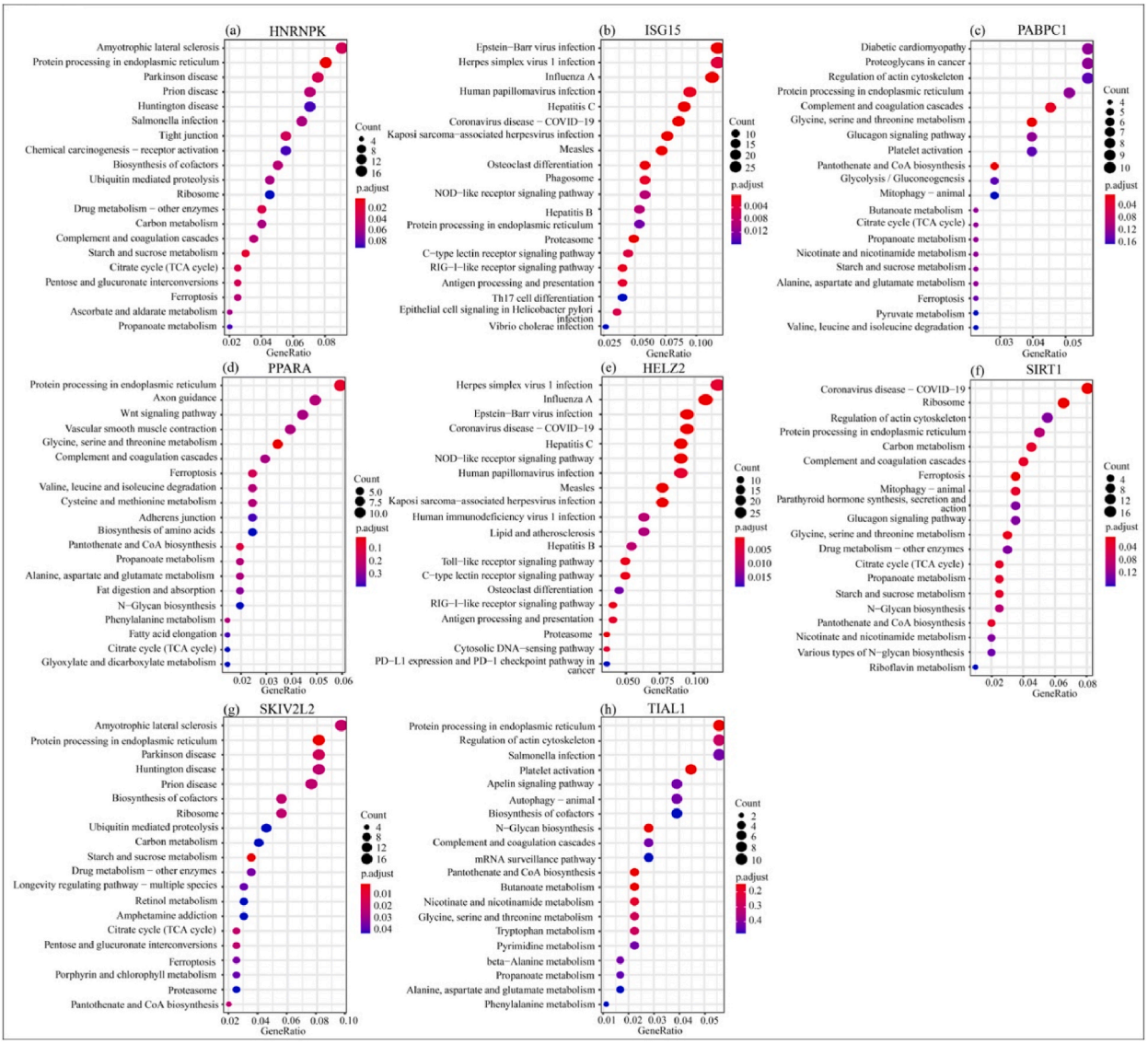

Fig. 8. Top 20 terms of the KEGG pathways of the indicated hub genes from GSE26625. (a–h) The top 20 terms of KEGG pathways associated with the eight hub genes (*HNRNPK*, *ISG15*, *PABPC1*, *PPARA*, *HELZ2*, *SIRT1*, *SKIV2L2*, *and TIAL1*).

association between ferroptosis and graft rejection as well as the loss of kidney transplantation, although further investigation is required to elucidate the underlying mechanisms [21].

Through WGCNA and PPI network analysis, we identified eight hub genes controlling the main biological pathways related to ACR following LT. In addition, *ISG15* and *HELZ2* were downregulated in the rejected group, while the other six genes were upregulated in the rejected group. *ISG15* was positively correlated with *HELZ2* but negatively correlated with the other six genes in all three GEO datasets, suggesting that *ISG15* played a key role during ACR following LT. According to the previous dataset-derived research, *ISG15* was associated with rejection [14]. With ROC analysis, three genes with the highest predicting potential were identified, including *HNRNPK*, *TIAL1*, and *PABPC1*. Notably, these three and the other five hub genes have not been reported in previous research on ACR following LT, while *PPARA* has been reported to be involved in tacrolimus metabolism among kidney transplantation patients [22]. Therefore, we hypothesize that these genes may serve as novel biomarkers for patients with ACR following LT, although further research is required to elucidate the underlying mechanisms.

Immune cells serve as the primary initiators of transplant rejection, and their role in regulating immune cell infiltration during ACR following LT remains unclear. Therefore, we first evaluated the immune cell infiltration in tissues obtained from GSE26625. The findings revealed that the main infiltrating cells consisted of NK cells, memory B cells, $CD4^{+}$memory T cells, Tregs, naïve B cells, neutrophils, mast cells, dendritic cells, and M1/M2-like macrophages. All these cell subsets are classical immune cell subsets involved in LT rejection [8]. We further investigated the correlation between the eight hub genes and infiltrating immune cells. The results

showed that all eight genes were closely related to infiltrating immune cells. In particular, *ISG15* was positively correlated with γδT cells, M1-like macrophages, and dendritic cells activated but negatively correlated with resting NK cells, resting $CD4^+$ memory T cells, and Tregs. Furthermore, *SIRT1* was positively correlated with resting NK cells, resting $CD4^+$ memory T cells, Tregs, naïve B cells, neutrophils, and M2-like macrophages but negatively correlated with γδT cells and memory B cells. Interestingly, the rejected group exhibited downregulation of *ISG15* and upregulation of *SIRT1*, and *ISG15* was negatively correlated with *SIRT1* in all three GEO datasets. Interferon-stimulated genes (ISGs) are induced by type I interferons during pathogen invasion [23]. Among these ISGs, the ubiquitin-like protein *ISG15* is one of the most powerful and fastest inducible proteins [24]. Previous studies have demonstrated that *ISG15* can be secreted by various cellular components, including particles, exosomes, neutrophil granules, secretory lysosomes, and apoptotic cells. Its immunomodulatory effects can stimulate NK cell proliferation, promote dendritic cell maturation, and activate macrophages to release IL-12. These actions contribute to the exacerbation of the inflammatory response [25]. Moreover, in the tumor microenvironment, *ISG15* induces M2-like tumor-associated macrophages to inhibit the cytotoxic T-lymphocyte response and facilitate tumor progression [26]. Recent studies have shown that *SIRT1* can inhibit M1-like macrophage polarization by deacetylating the transcription factor *IRF8* [27,28]. These findings suggest a regulatory role of both *ISG15* and *SIRT1* in macrophage polarization. Previous studies have shown that increasing the number of $CD4^+$ Tregs improves tolerance in liver transplantation [12,29,30], and studies have proven that both *ISG15* and *SIRT1* can regulate Tregs in a positive or negative manner [31,32]. These results are consistent with our findings. However, the potential modulation of macrophage polarization, Tregs, and NK cells by ISG15 and SIRT1 in the context of ACR following LT and their associations remain unexplored.

The results of KEGG analysis of the eight hub genes showed that the pathways associated with ferroptosis, protein processing in the endoplasmic reticulum, complement and coagulation, and the RIG-I/NOD/Toll-like receptor signaling pathway showed the most significant correlation with ACR. Ferroptosis was expected to be involved in ACR following LT, and it was also found to be associated with the hub genes *ISG15, HNRNPK, PABPC1, SKIV2L2, SIRT1*, and *PPARA*. These results suggest a significant correlation between the ferroptosis pathway and ACR following LT. In solid organ transplantation, increasing evidence from both experimental and human studies suggests that Toll-like receptor (TLR) activation is involved in the innate immune recognition of allografts and is closely associated with acute allograft rejection after LT [33,34]. Therefore, close attention should be devoted to these signaling pathways for the development of new drugs and therapeutic strategies for ACR following LT.

In summary, we identified eight hub genes and their potential pathways and infiltrating immune cells involved in ACR following LT with omics-based data in the dry lab. Our study has certain limitations, as the results were validated by bioinformatics tools in the dry lab without wet lab validation from our cohort study. In addition, the molecular mechanisms underlying these hub genes, potential pathways, and the involvement of infiltrating immune cells in ACR of LT remain to be explored. In future studies, the results obtained will be further validated, and the potential use of these hub genes as rejection biomarkers will be evaluated. However, these preliminary findings have important implications for guiding future mechanism research and improving the treatment of ACR following LT.

Data availability

The data used in this article were accessed from the GEO database (https://www.ncbi.nlm. nih.gov/geo/, GSE26622, GSE26625, and GSE52420). The data generated in this research will be shared upon reasonable request to the corresponding author.

CRediT authorship contribution statement

Cheng Zhang: Writing – original draft, Methodology, Investigation, Data curation. **Jun-Ze Chen:** Writing – original draft, Methodology, Investigation, Formal analysis, Data curation. **Kun Dong:** Writing – original draft, Data curation, Conceptualization. **Yong-Yuan Jian:** Writing – original draft, Methodology, Formal analysis. **Kai-Yong Huang:** Writing – original draft, Methodology, Formal analysis. **Rui-Ling Su:** Writing – original draft, Investigation, Formal analysis. **Xue-Lin Tan:** Writing – original draft, Visualization, Methodology, Investigation. **Guan-Dou Yuan:** Writing – original draft, Visualization, Investigation, Formal analysis. **Yu-yan Lan:** Writing – original draft, Investigation, Data curation. **Song-Qing He:** Writing – review & editing. **Chun-Qiang Dong:** Writing – review & editing, Conceptualization.

Declaration of competing interest

The authors declare the following financial interests/personal relationships which may be considered as potential competing interests:Chun-Qiang Dong reports financial support was provided by The First Affiliated Hospital of Guangxi Medical University. Song-Qing He reports financial support was provided by The First Affiliated Hospital of Guangxi Medical University. Chun-Qiang Dong reports a relationship with The First Affiliated Hospital of Guangxi Medical University that includes: funding grants. Song-Qing He reports a relationship with The First Affiliated Hospital of Guangxi Medical University that includes: funding grants. No other conflicts of interest. If there are other authors, they declare that they have no known competing financial interests or personal relationships that could have appeared to influence the work reported in this paper.

Acknowledgments

This work was supported in part by Key topics of Funding in 2023 under the "14th Five-Year Plan" of Guangxi Education Science

(Category A) (2023A099), Guangxi Natural Science Foundation (Youth Science Foundation Project) (2023GXNSFBA026116), Guangxi Key Research and Development Plan, China (2018AD03001), the Special Project of Government Guiding Local Science and Technology Development (ZY201980011), and the Key Laboratory Base of Liver Injury and Repair of the First Affiliated Hospital of Guangxi Medical University (YYZS2020001). We thank Essentialslink Language Services (www.essentialslink.cn) for its linguistic assistance during the preparation of this manuscript.

Abbreviations

Abbreviation	Detail
ACR	Acute cellular rejection
AMR	Antibody-mediated rejection
BP	Biological process
CC	Cellular component
DEG	Differentially expressed gene
GEO	Gene Expression Omnibus
GO	Gene Ontology
ISGs	Interferon-stimulated genes
KEGG	Kyoto Encyclopedia of Genes and Genomes
LT	Liver transplantation
ME	Module eigengene
MF	Molecular function
PPI	Protein-protein interaction
ROC	Receiver operating characteristic
TCMR	T cell-mediated rejection
TLR	Toll-like receptor
Tregs	T regulatory cells
WGCNA	Weighted gene co-expression network analysis

Appendix A. Supplementary data

Supplementary data to this article can be found online at https://doi.org/10.1016/j.heliyon.2024.e33359.

References

[1] J. Levitsky, et al., Acute rejection increases risk of graft failure and death in recent liver transplant recipients, Clin. Gastroenterol. Hepatol. 15 (4) (2017) 584–593 e2.
[2] M. Rodríguez-Perálvarez, et al., Biopsy-proven acute cellular rejection as an efficacy endpoint of randomized trials in liver transplantation: a systematic review and critical appraisal, Transpl. Int. 29 (9) (2016) 961–973.
[3] B.T. Lee, M.I. Fiel, T.D. Schiano, Antibody-mediated rejection of the liver allograft: an update and a clinico-pathological perspective, J. Hepatol. 75 (5) (2021) 1203–1216.
[4] T.J. Kohut, J.F. Barandiaran, B.J. Keating, Genomics and liver transplantation: genomic biomarkers for the diagnosis of acute cellular rejection, Liver Transplant. 26 (10) (2020) 1337–1350.
[5] A. Regev, et al., Sampling error and intraobserver variation in liver biopsy in patients with chronic HCV infection, Am. J. Gastroenterol. 97 (10) (2002) 2614–2618.
[6] T.A. Alten, et al., Safety and performance of liver biopsies in liver transplant recipients, Clin. Transplant. 28 (5) (2014) 585–589.
[7] Y. Tang, et al., Clinical characteristics of immune tolerance after pediatric liver transplantation, BMC Surg. 22 (1) (2022) 102.
[8] V. Ronca, et al., The immunological basis of liver allograft rejection, Front. Immunol. 11 (2020) 2155.
[9] R. Alfaro, et al., Computational prediction of biomarkers, pathways, and new target drugs in the pathogenesis of immune-based diseases regarding kidney transplantation rejection, Front. Immunol. 12 (2021).
[10] L. Toti, et al., Towards tolerance in liver transplantation, Best Pract. Res. Clin. Gastroenterol. 54–55 (2021) 101770.
[11] J. Neuberger, Immunosuppression in gastroenterology and hepatology, Best Pract. Res. Clin. Gastroenterol. 54–55 (2021) 101758.
[12] Z. Beyzaei, A. Shojazadeh, B. Geramizadeh, The role of regulatory T cells in liver transplantation, Transpl. Immunol. 70 (2022) 101512.
[13] F. Bohne, et al., Intra-graft expression of genes involved in iron homeostasis predicts the development of operational tolerance in human liver transplantation, J. Clin. Invest. 122 (1) (2012) 368–382.
[14] F. Bohne, et al., HCV-induced immune responses influence the development of operational tolerance after liver transplantation in humans, Sci. Transl. Med. 6 (242) (2014) 242ra81.
[15] R. Alfaro, et al., Computational prediction of biomarkers, pathways, and new target drugs in the pathogenesis of immune-based diseases regarding kidney transplantation rejection, Front. Immunol. 12 (2021) 800968.
[16] X. Chen, et al., Inhibition of autophagy prolongs recipient survival through promoting CD8(+) T cell apoptosis in a rat liver transplantation model, Front. Immunol. 10 (2019) 1356.
[17] D. Degli Esposti, et al., Ischemic preconditioning induces autophagy and limits necrosis in human recipients of fatty liver grafts, decreasing the incidence of rejection episodes, Cell Death Dis. 2 (2011) e111.
[18] X. Sui, et al., RSL3 drives ferroptosis through GPX4 inactivation and ROS production in colorectal cancer, Front. Pharmacol. 9 (2018) 1371.
[19] N. Yamada, et al., Iron overload as a risk factor for hepatic ischemia-reperfusion injury in liver transplantation: potential role of ferroptosis, Am. J. Transplant. 20 (6) (2020) 1606–1618.
[20] L. Wu, et al., miR-124-3p delivered by exosomes from heme oxygenase-1 modified bone marrow mesenchymal stem cells inhibits ferroptosis to attenuate ischemia-reperfusion injury in steatotic grafts, J. Nanobiotechnol. 20 (1) (2022) 196.
[21] Z. Fan, et al., A ferroptosis-related gene signature for graft loss prediction following renal allograft, Bioengineered 12 (1) (2021) 4217–4232.

[22] J.B.F. Everton, et al., CYP3A5 and PPARA genetic variants are associated with low trough concentration to dose ratio of tacrolimus in kidney transplant recipients, Eur. J. Clin. Pharmacol. 77 (6) (2021) 879–886.
[23] W.M. Schneider, M.D. Chevillotte, C.M. Rice, Interferon-stimulated genes: a complex web of host defenses, Annu. Rev. Immunol. 32 (2014) 513–545.
[24] S.D. Der, et al., Identification of genes differentially regulated by interferon alpha, beta, or gamma using oligonucleotide arrays, Proc. Natl. Acad. Sci. U. S. A. 95 (26) (1998) 15623–15628.
[25] D. Bogunovic, et al., Mycobacterial disease and impaired IFN-gamma immunity in humans with inherited ISG15 deficiency, Science 337 (6102) (2012) 1684–1688.
[26] R.H. Chen, et al., Tumor cell-secreted ISG15 promotes tumor cell migration and immune suppression by inducing the macrophage M2-like phenotype, Front. Immunol. 11 (2020) 594775.
[27] Y. Jia, et al., IRF8 is the target of SIRT1 for the inflammation response in macrophages, Innate Immun. 23 (2) (2017) 188–195.
[28] F. Xu, et al., Angiogenic deficiency and adipose tissue dysfunction are associated with macrophage malfunction in SIRT1-/- mice, Endocrinology 153 (4) (2012) 1706–1716.
[29] A. Sánchez-Fueyo, et al., Applicability, safety, and biological activity of regulatory T cell therapy in liver transplantation, Am. J. Transplant. 20 (4) (2020) 1125–1136.
[30] K. Wang, et al., Different phenotypes of CD4(+)CD25(+)Foxp3(+) regulatory T cells in recipients post liver transplantation, Int. Immunopharm. 69 (2019) 194–201.
[31] H.S. Kwon, et al., Three novel acetylation sites in the Foxp3 transcription factor regulate the suppressive activity of regulatory T cells, J. Immunol. 188 (6) (2012) 2712–2721.
[32] I. Pacella, et al., ISG15 protects human Tregs from interferon alpha-induced contraction in a cell-intrinsic fashion, Clin Transl Immunology 9 (12) (2020) e1221.
[33] D.R. Goldstein, Toll like receptors and acute allograft rejection, Transpl. Immunol. 17 (1) (2006) 11–15.
[34] J.F. Deng, et al., The role of toll-like receptors 2 and 4 in acute allograft rejection after liver transplantation, Transplant. Proc. 39 (10) (2007) 3222–3224.